Supporting Information

A Metal-Organic-Framework-Derived $(Zn_{0.95}Cu_{0.05})_{0.6}Cd_{0.4}S$ Solid Solution as Efficient Photocatalyst for Hydrogen Evolution Reaction

Jing Liu,[†] Jianrui Feng,[†] Lele Lu,[†] Boyuan Wu,[†] Peng Ren,*[,‡] Wei Shi*[,†] and Peng Cheng[†]

[†]Key Laboratory of Advanced Energy Materials Chemistry (MOE), College of Chemistry, Nankai University, Tianjin 300071, China

[‡]School of Science, Harbin Institute of Technology (Shenzhen), Shenzhen 518055, China

*E-mail: shiwei@nankai.edu.cn (W.S.)

*E-mail: renpeng@hit.edu.cn (P.R.)

Table of Contents

EXPERIMENTAL SECTION		S-4-S-6
Figure S1	SEM image of Cd-MOF.	S-7
Figure S2	PXRD patterns of $(Zn_{1-x}Cu_x)$-MOF.	S-7
Figure S3	PXRD patterns of $(Zn_{1-x}Cu_x)S$ solid solutions.	S-7
Figure S4	Comparison of photocatalytic HER rates with $(Zn_{1-x}Cu_x)S$ heterojunctions under visible-light irradiation.	S-8
Figure S5	PXRD patterns of $(Zn_{0.95}Cu_{0.05})_{1-x}Cd_x$-MOF.	S-8

Figure S6	TG curves of $(Zn_{0.95}Cu_{0.05})_{1-x}Cd_x$-MOF.	S-8
Figure S7	PXRD patterns of $(Zn_{1-x}Cd_x)S$ solid solutions.	S-9
Figure S8	Elemental mapping images of $(Zn_{0.95}Cu_{0.05})$-MOF.	S-9
Figure S9	Elemental mapping images of $(Zn_{0.95}Cu_{0.05})_{0.8}Cd_{0.2}$-MOF.	S-9
Figure S10	Elemental mapping images of $(Zn_{0.95}Cu_{0.05})_{0.6}Cd_{0.4}$-MOF.	S-10
Figure S11	Elemental mapping images of $(Zn_{0.95}Cu_{0.05})_{0.4}Cd_{0.6}$-MOF.	S-10
Figure S12	Elemental mapping images of $(Zn_{0.95}Cu_{0.05})_{0.2}Cd_{0.8}$-MOF.	S-10
Figure S13	Elemental mapping images of Cd-MOF.	S-11
Figure S14	EDS patterns of $(Zn_{0.95}Cu_{0.05})$-MOF (a), $(Zn_{0.95}Cu_{0.05})_{0.8}Cd_{0.2}$-MOF (b), $(Zn_{0.95}Cu_{0.05})_{0.6}Cd_{0.4}$-MOF (c), $(Zn_{0.95}Cu_{0.05})_{0.4}Cd_{0.6}$-MOF (d), $(Zn_{0.95}Cu_{0.05)0.2}Cd_{0.8}$-MOF (e) and Cd-MOF (f).	S-11
Figure S15	SEM images of $(Zn_{0.95}Cu_{0.05})S$ (a), $(Zn_{0.95}Cu_{0.05})_{0.8}Cd_{0.2}S$ (b), $(Zn_{0.95}Cu_{0.05})_{0.6}Cd_{0.4}S$ (c), $(Zn_{0.95}Cu_{0.05})_{0.4}Cd_{0.6}S$ (d), $(Zn_{0.95}Cu_{0.05})_{0.2}Cd_{0.8}S$ (e) and CdS (f).	S-12
Figure S16	(a) XPS full-spectrum of $(Zn_{0.95}Cu_{0.05})_{0.4}Cd_{0.6}S$, (b) Cu 2p spectrum, (c) Zn 2p spectrum, (d) Cd 3d spectrum, (e) S 2p spectrum and (f) C1s spectrum.	S-13
Figure S17	Nitrogen adsorption/desorption isotherms of CdS and $(Zn_{0.95}Cu_{0.05})_{0.6}Cd_{0.4}S$.	S-14
Figure S18	BJH pore size distribution from adsorption branch of CdS and $(Zn_{0.95}Cu_{0.05})_{0.6}Cd_{0.4}S$.	S-14
Figure S19	The bandgaps of $(Zn_{0.95}Cu_{0.05})S$ (a), $(Zn_{0.95}Cu_{0.05})_{0.8}Cd_{0.2}S$ (b), $(Zn_{0.95}Cu_{0.05})_{0.6}Cd_{0.4}S$ (c), $(Zn_{0.95}Cu_{0.05})_{0.4}Cd_{0.6}S$ (d), $(Zn_{0.95}Cu_{0.05})_{0.2}Cd_{0.8}S$ (e) and CdS (f) calculated according to the Kubelka-Munk (KM) method.	S-15
Figure S20	Mechanism of $(Zn_{0.95}Cu_{0.05})_{0.6}Cd_{0.4}S$ and CdS for photocatalytic hydrogen production.	S-15
Figure S21	Decay curves and luminescent lifetimes of $(Zn_{0.95}Cu_{0.05})S$	S-16

	(a), $(Zn_{0.95}Cu_{0.05})_{0.8}Cd_{0.2}S$ (b), $(Zn_{0.95}Cu_{0.05})_{0.6}Cd_{0.4}S$ (c), $(Zn_{0.95}Cu_{0.05})_{0.4}Cd_{0.6}S$ (d), $(Zn_{0.95}Cu_{0.05})_{0.2}Cd_{0.8}S$ (e) and CdS (f).	
Figure S22	PXRD patterns of $(Zn_{1-x}Cd_x)$-MOF.	S-16
Figure S23	PXRD patterns of $(Zn_{1-x}Cd_x)S$ solid solutions.	S-17
Figure S24	Photocatalytic performance of $(Zn_{1-x}Cd_x)S$ solid solutions.	S-17
Figure S25	Comparison of photocatalytic HER of $(Zn_{1-x}Cd_x)S$ solid solutions.	S-17
Figure S26	XRD patterns of $(Zn_{0.95}Cu_{0.05})_{0.6}Cd_{0.4}S$ collected after photocatalytic hydrogen evolution experiment.	S-18
Figure S27	TEM image and elemental mapping images of $(Zn_{0.95}Cu_{0.05})_{0.6}Cd_{0.4}S$ after photocatalytic hydrogen evolution experiment.	S-18
Figure S28	Solid solution model of $(Zn_{0.95}Cu_{0.05})_{0.6}Cd_{0.4}S$	S-19
Table S1	The experimental data of ICP-OES and elemental analyses of $(Zn_{0.95}Cu_{0.05})_{1-x}Cd_xS$ solid solutions.	S-19
Table S2	The energy positions of conduction and valence bands of samples. (ECB based on Mott-Schottky plots)	S-20
Table S3.	Comparison of the H_2-production rates of CuS_x cocatalysts solid solution for water splitting	S-20
Table S4	Comparison of the H_2-production rates of CdS-based solid solution heterojunction for water splitting.	S-21-S-22
Reference		S-23-S-25

EXPERIMENTAL SECTION

Preparation of $(Zn_{0.95}Cu_{0.05})_{1-x}Cd_x$-MOF. $Cd(NO_3)_2·4H_2O$ (x mmol), $Cu(NO_3)_2·3H_2O$ (y mmol), $Zn(NO_3)_2·6H_2O$ (19y mmol), (x / 20y = 0, 1/4, 2/3, 3/2, 4/1, 1, x + 20y = 1.69), and PVP (1.0 g) were dissolved in DMF (30 mL) followed by addition of a DMF solution (30 mL) containing H_2bdc (0.501 g, 3.02 mmol) and PVP (1.0 g). After ultrasonic treatment, the solution was refluxed at 115 ºC for 5 h. After natural refrigeration, the products were obtained via centrifugation, washed with DMF and methanol three times, respectively and then dried at 50 °C overnight. Finally, the products $(Zn_{0.95}Cu_{0.05})_{1-x}Cd_x$-MOF ($(Zn_{0.95}Cu_{0.05})$-MOF, $(Zn_{0.95}Cu_{0.05})_{0.8}Cd_{0.2}$-MOF, $(Zn_{0.95}Cu_{0.05})_{0.6}Cd_{0.4}$-MOF, $(Zn_{0.95}Cu_{0.05})_{0.4}Cd_{0.6}$-MOF, $(Zn_{0.95}Cu_{0.05})_{0.2}Cd_{0.8}$-MOF and Cd-MOF) were obtained.

Preparation of $Zn_{1-x}Cd_x$-MOF. Similar to the synthetic method of $(Zn_{0.95}Cu_{0.05})_{1-x}Cd_x$-MOF, while $Cu(NO_3)_2·3H_2O$ was replaced with $Zn(NO_3)_2·6H_2O$ absolutely, and the products Zn_xCd_{1-x}-MOF (Zn-MOF, $Zn_{0.8}Cd_{0.2}$-MOF, $Zn_{0.6}Cd_{0.4}$-MOF, $Zn_{0.4}Cd_{0.6}$-MOF, $Zn_{0.2}Cd_{0.8}$-MOF and Cd-MOF) were obtained.

Materials characterization. The as-prepared nanocatalysts were characterized via powder X-ray diffraction (PXRD, D/Max-2500 X-ray diffractometer using Cu Kα radiation, λ = 1.54056 Å, at a scan speed of 5° min^{-1} in the range 2θ = 10-80°), thermogravimetric analyses (TGA, Labsys NETZSCH TG 209 Setaram apparatus with increasing rate of 10 °C min^{-1} from 25 to 800 °C under N_2 atmosphere), X-ray photoelectron spectroscopy (XPS, Axis Ultra DLD), UV-vis spectroscopy (Jasco V-570 spectrophotometer), photoluminescence spectroscopy (PL, Agilent Cary

Eclipse spectrophotometer), elemental analyses (C, H and N, Perkin-Elmer 2400-II CHNS/O analyzer), inductively coupled plasma optical emission spectrometry (ICP-OES, Spectro-Blue), scanning electron microscopy (SEM, JEOL JSM 7500F), transmission electron microscopy (TEM, FEI Tecnai G20), and nitrogen sorption isotherms measurement (Autosorb-IQ2 (Quantachrome Instruments), 77 K). The photoelectrochemical experiments were carried out in a CHI660D electrochemical system with a standard three-electrode configuration containing a Pt flake as the counter electrode, an Ag/AgCl reference electrode, and the synthesized catalysts as the working electrode in 0.1 M Na_2SO_4 solution. The working electrode was prepared on the basis of the literature.[1] A 300 W Xe lamp equipped with a 420 nm cut-off filter was used as the light source.

Photocatalytic activity tests. The photocatalytic activity for water splitting tests was conducted using a 300 W Xe lamp (PLS-SXE 300C, Beijing Perfect Light Co. Ltd, China, wavelength: 320-780 nm) as light source. The reactor was linked to a closed gas circulation and evacuation system. A typical hydrogen production experiment was performed by dispersing 50 mg catalyst in an aqueous solution involving $Na_2S{\cdot}9H_2O$ (35.0 mmol, 8.4 g) and Na_2SO_3 (25.0 mmol, 3.15 g) as the sacrificial electron donors. The reaction system was sealed and removed residual air thoroughly. The reaction system was investigated under irradiation though a 420 nm cut-off filter with a settled distance (10 cm), and the system temperature was maintained at 5 °C via water circulation under continuous magnetic stirring. The amount of gas product was

detected via gas chromatography using a thermal conductive detector (TCD) with N_2 as the carrier gas.

Calculation Method and Models. In this work, density functional theory (DFT) based calculations were implemented by the Vienna ab initio simulation package (VASP) to optimize the structures and calculate the projected band structure and projected density of states (PDOS). The ion-electron interactions were depicted by projector augmented waves (PAW)[2] when the function of Perdew, Burke and Ernzerhof (PBE)[3] based on the generalized gradient approximation (GGA) was adopted to describe the exchange and correlation potential. In this calculation, 7*7*7 Monkhorst-Pack[4] sampled k points were used and a cut-off energy of 400 eV was adopted. The threshold of convergence was set to 1×10^{-5} eV and 0.01 eV/Å for the self-consistent field (SCF) and ion steps, respectively. It should be noted that the method of DFT always underestimates the band gaps of semiconductors, though the qualitative conclusions from DFT calculations are usually reliable to illustrate the trends. The high-symmetry points in band structure are G (0, 0, 0), A (0, 0, 0.5), H (-0.333, 0.667, 0.5), K (-0.333, 0.667, 0), M (0, 0.5, 0) and L (0, 0.5, 0.5).

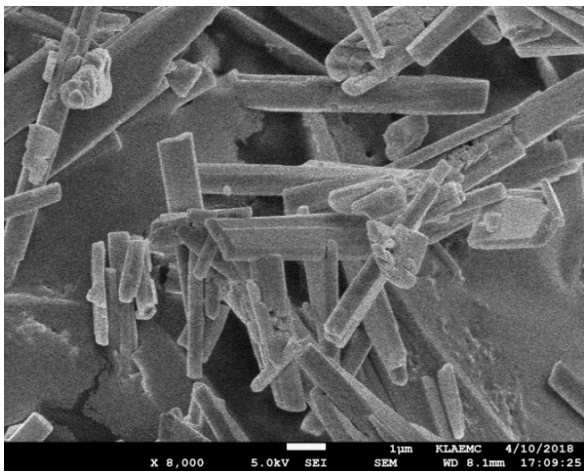

Figure S1 SEM image of Cd-MOF.

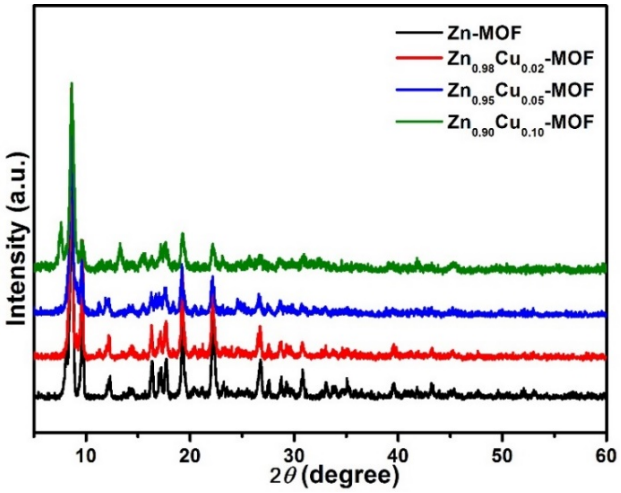

Figure S2 PXRD patterns of $(Zn_{1-x}Cu_x)$-MOF (x=0, 0.02, 0.05, 0.10).

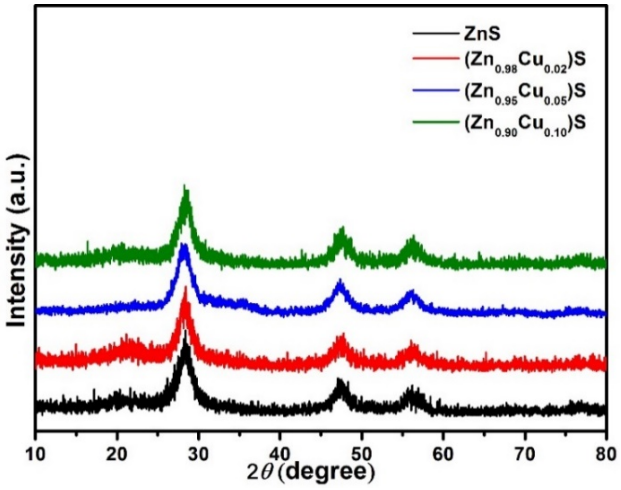

Figure S3 PXRD patterns of $(Zn_{1-x}Cu_x)S$ solid solutions (x=0, 0.02, 0.05, 0.10).

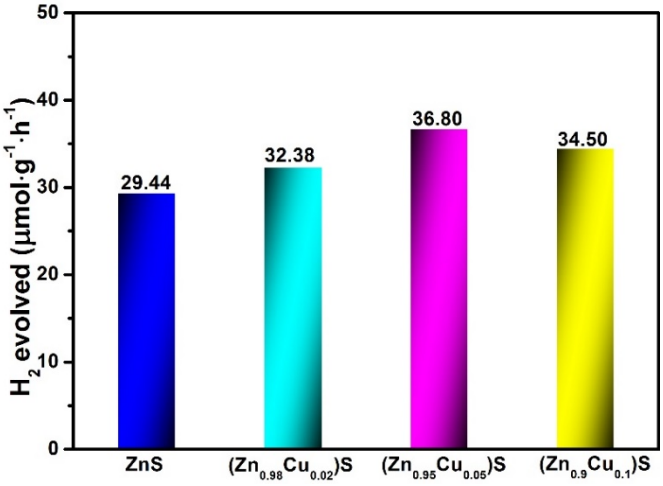

Figure S4 Comparison of photocatalytic HER rates with $(Zn_{1-x}Cu_x)S$ solid solutions under visible-light irradiation.

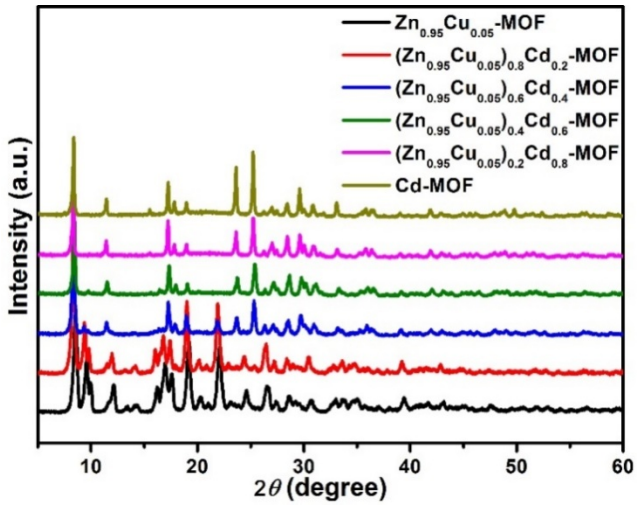

Figure S5 PXRD patterns of $(Zn_{0.95}Cu_{0.05})_{1-x}Cd_x$-MOF.

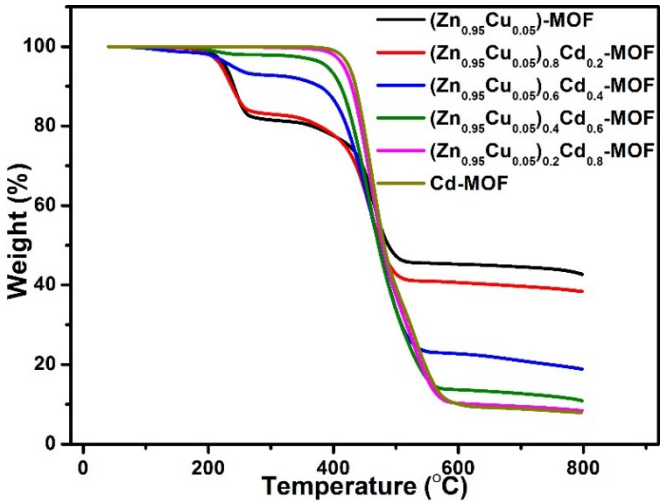

Figure S6 TGA curves of $(Zn_{0.95}Cu_{0.05})_{1-x}Cd_x$-MOF.

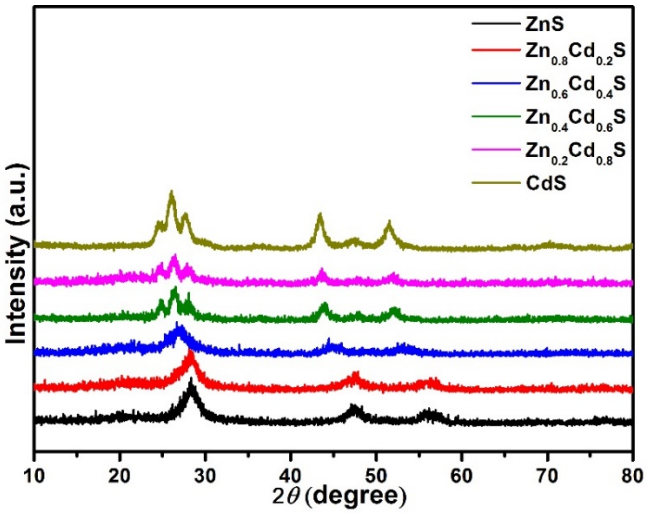

Figure S7 PXRD patterns of $(Zn_{1-x}Cd_x)S$ solid solutions (x=0, 0.2, 0.4, 0.6, 0.8, 1.0).

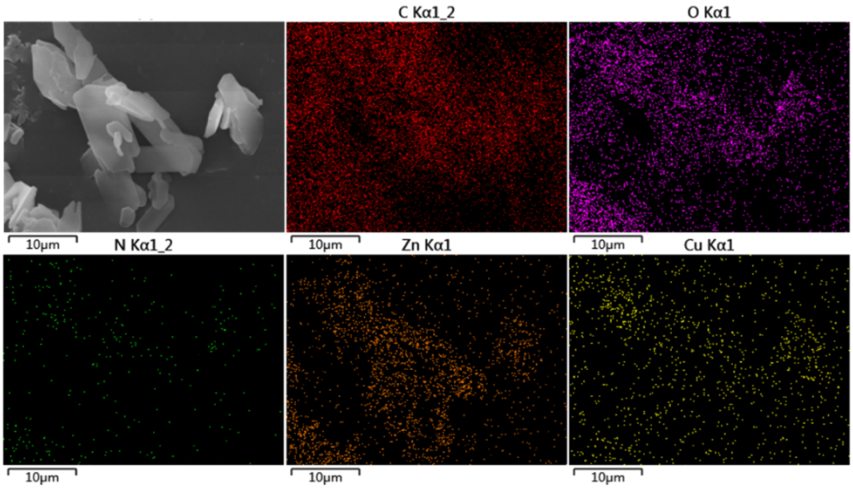

Figure S8 Elemental mapping images of $(Zn_{0.95}Cu_{0.05})$-MOF.

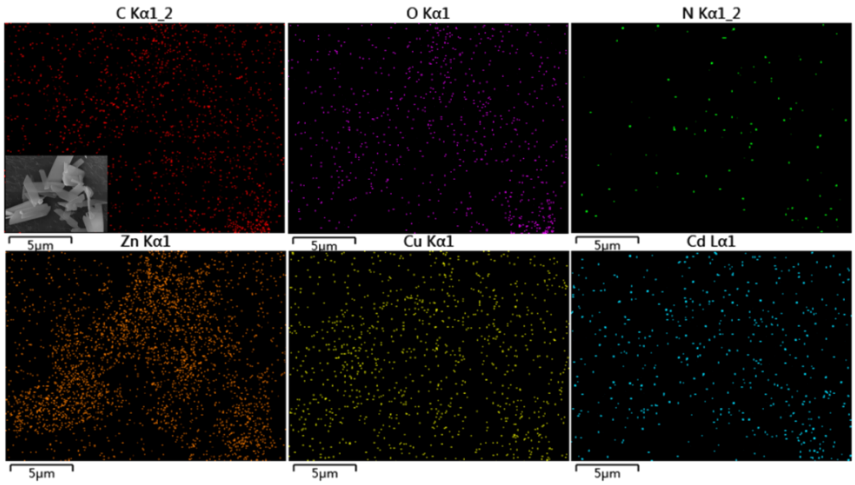

Figure S9 Elemental mapping images of $(Zn_{0.95}Cu_{0.05})_{0.8}Cd_{0.2}$-MOF.

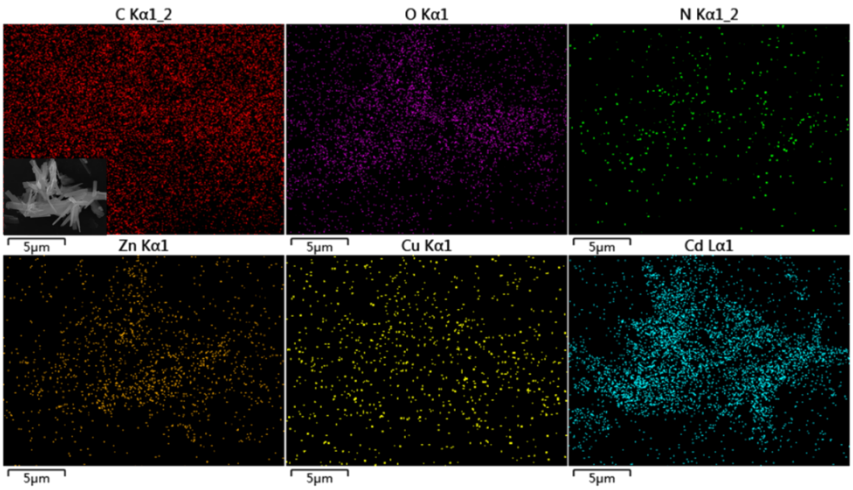

Figure S10 Elemental mapping images of $(Zn_{0.95}Cu_{0.05})_{0.6}Cd_{0.4}$-MOF.

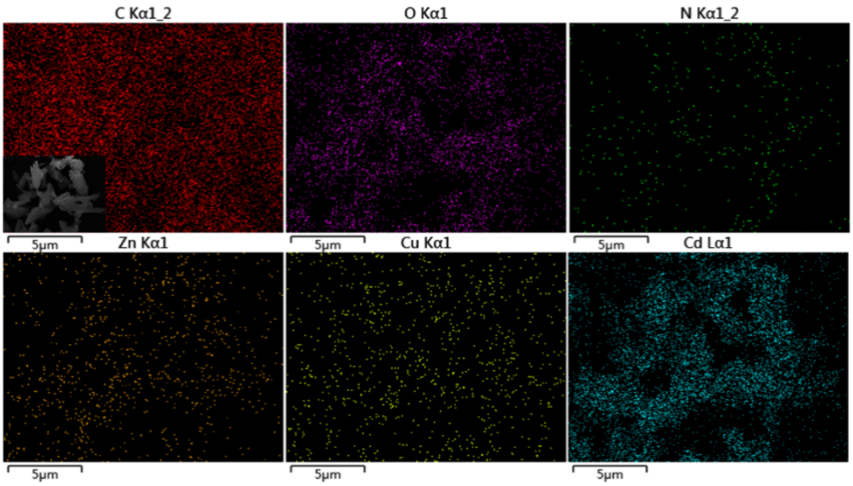

Figure S11 Elemental mapping images of $(Zn_{0.95}Cu_{0.05})_{0.4}Cd_{0.6}$-MOF.

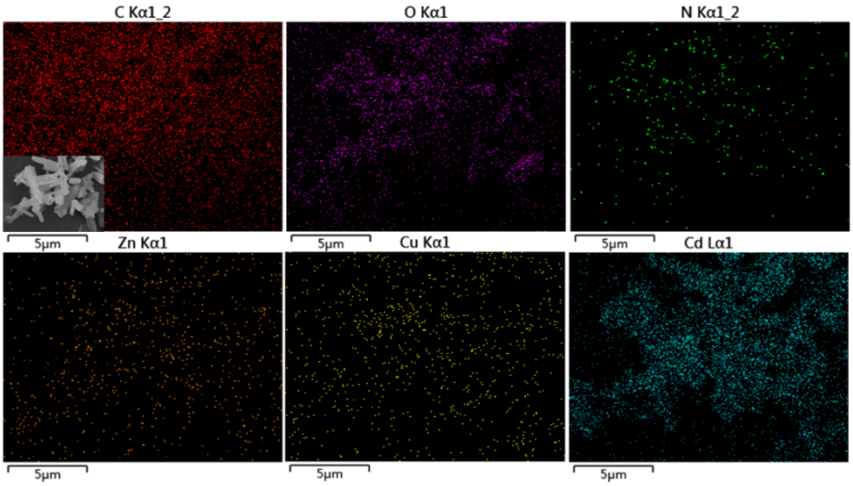

Figure S12 Elemental mapping images of $(Zn_{0.95}Cu_{0.05})_{0.2}Cd_{0.8}$-MOF.

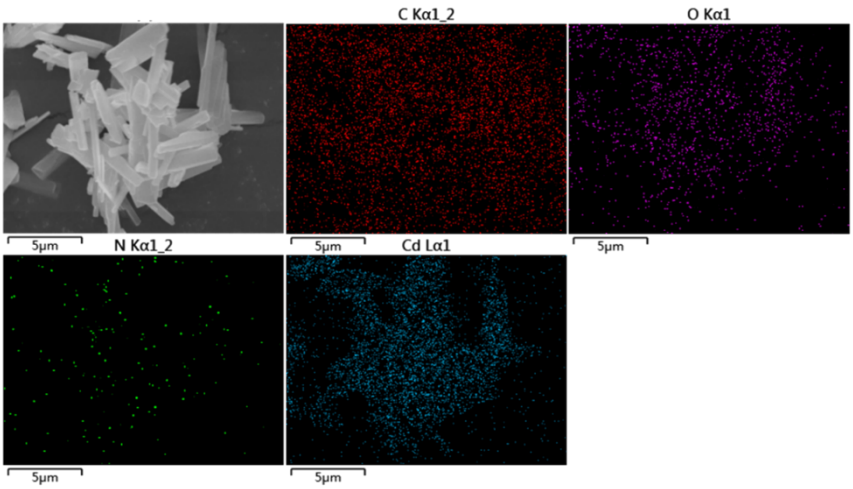

Figure S13 Elemental mapping images of Cd-MOF.

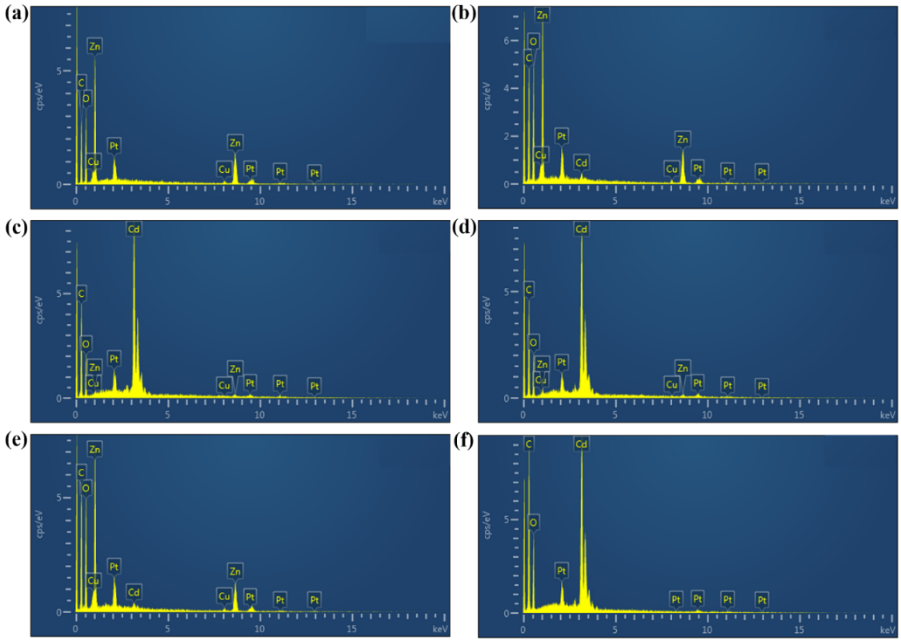

Figure S14 EDS patterns of $(Zn_{0.95}Cu_{0.05})$-MOF (a), $(Zn_{0.95}Cu_{0.05})_{0.8}Cd_{0.2}$-MOF (b), $(Zn_{0.95}Cu_{0.05})_{0.6}Cd_{0.4}$-MOF (c), $(Zn_{0.95}Cu_{0.05})_{0.4}Cd_{0.6}$-MOF (d), $(Zn_{0.95}Cu_{0.05})_{0.2}Cd_{0.8}$-MOF (e) and Cd-MOF (f). The preparation techniques for EDX as follow: Firstly, stick the conductive adhesive tape on the sample holder; secondly, sprinkle the powder sample evenly on it and blow off the non-stick powder with an ear wash ball, and then spray a conductive layer (Pt) for testing.

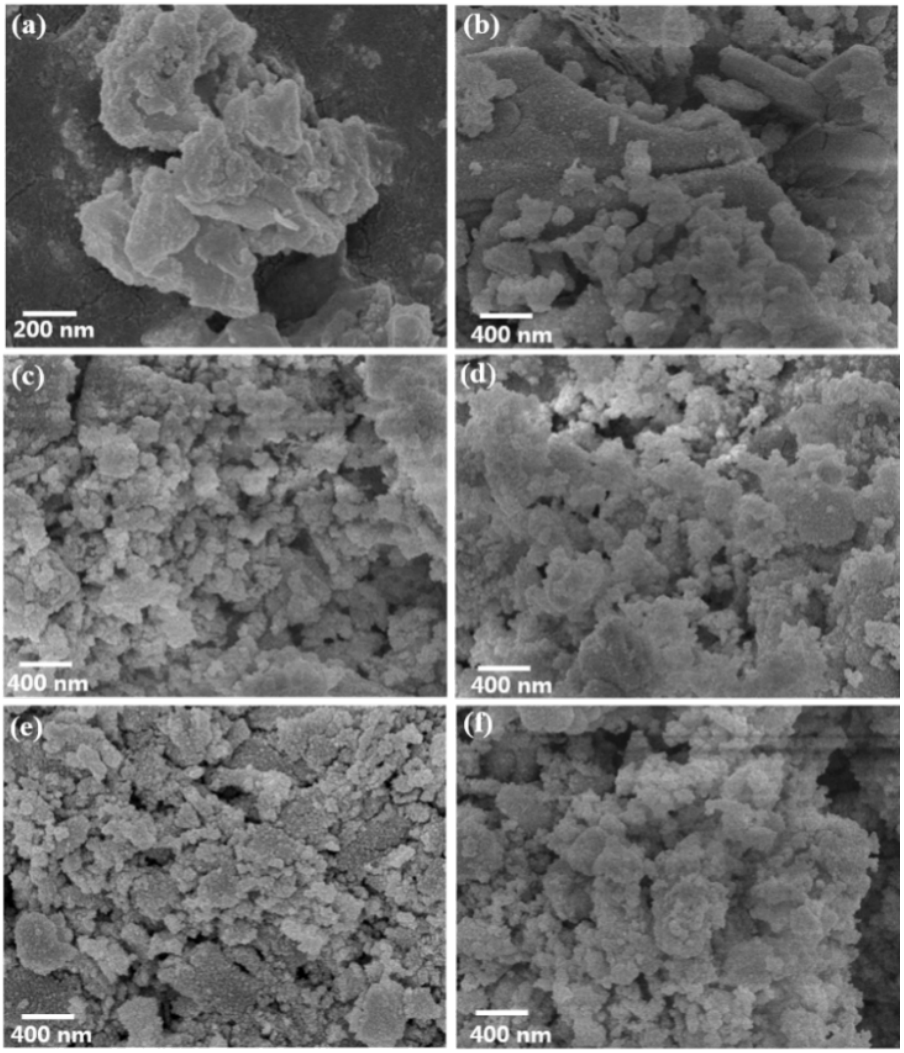

Figure S15 SEM images of $(Zn_{0.95}Cu_{0.05})S$ (a), $(Zn_{0.95}Cu_{0.05})_{0.8}Cd_{0.2}S$ (b), $(Zn_{0.95}Cu_{0.05})_{0.6}Cd_{0.4}S$ (c), $(Zn_{0.95}Cu_{0.05})_{0.4}Cd_{0.6}S$ (d), $(Zn_{0.95}Cu_{0.05})_{0.2}Cd_{0.8}S$ (e) and CdS (f).

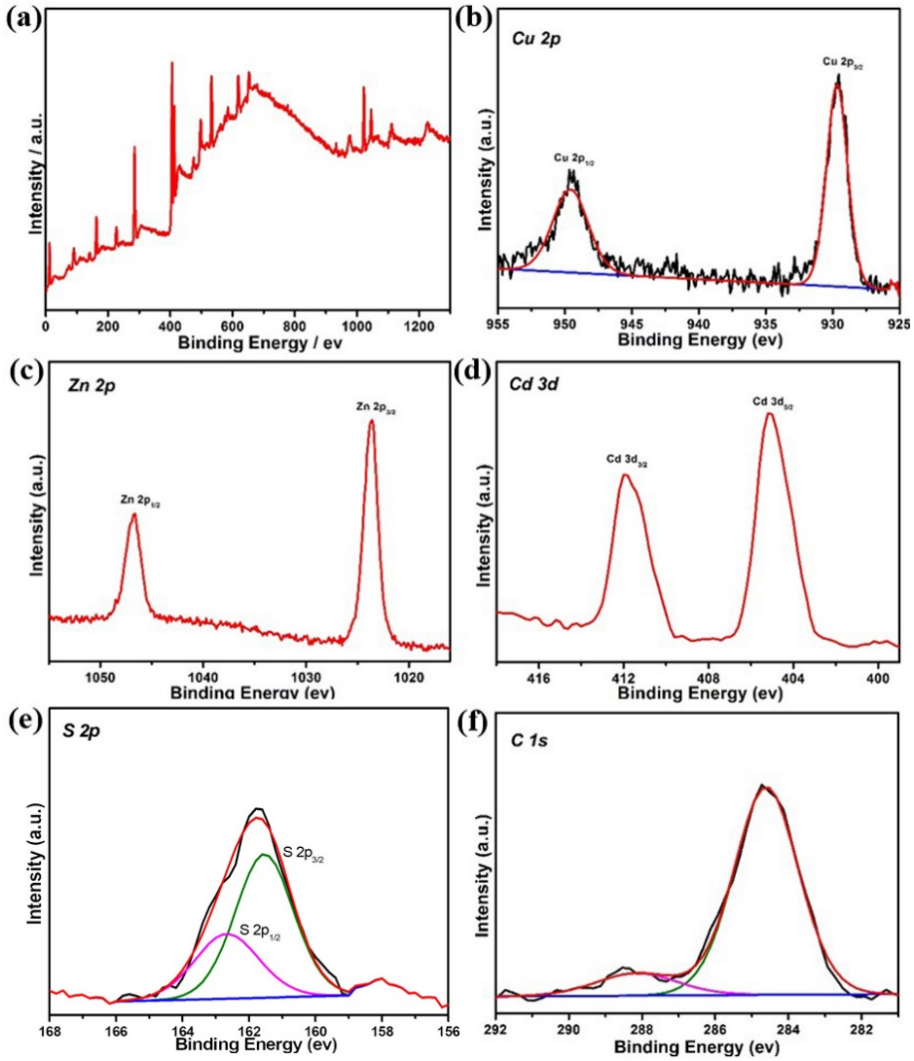

Figure S16 (a) XPS full-spectrum of $(Zn_{0.95}Cu_{0.05})_{0.6}Cd_{0.4}S$, (b) Cu 2p spectrum, (c) Zn 2p spectrum, (d) Cd 3d spectrum, (e) S 2p spectrum and (f) C1s spectrum.

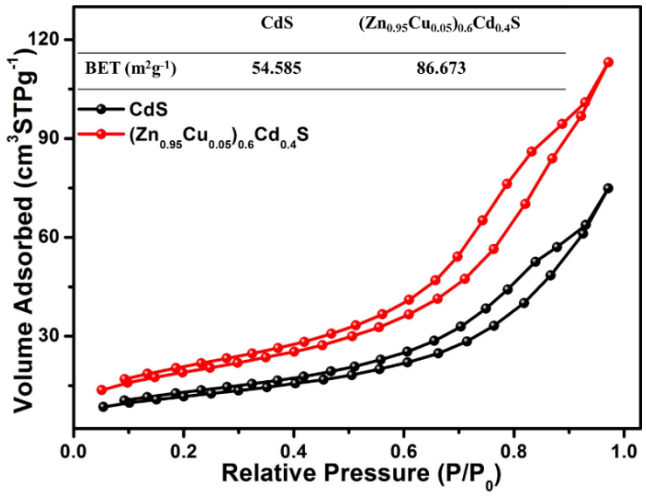

Figure S17 Nitrogen adsorption/desorption isotherms of CdS and $(Zn_{0.95}Cu_{0.05})_{0.6}Cd_{0.4}S$.

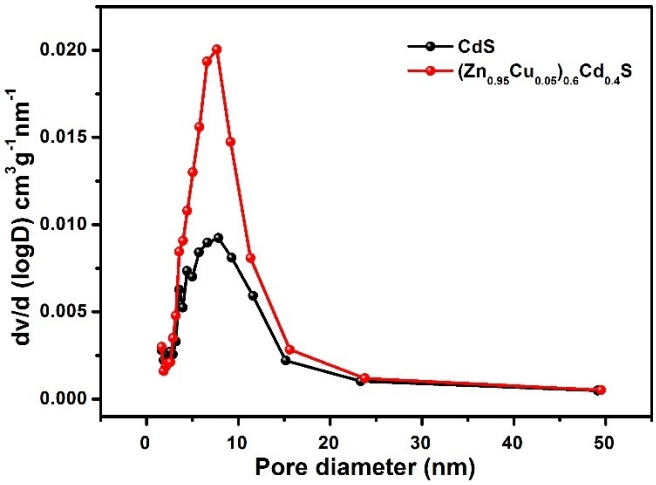

Figure S18 BJH pore size distribution from adsorption branch of CdS and $(Zn_{0.95}Cu_{0.05})_{0.6}Cd_{0.4}S$.

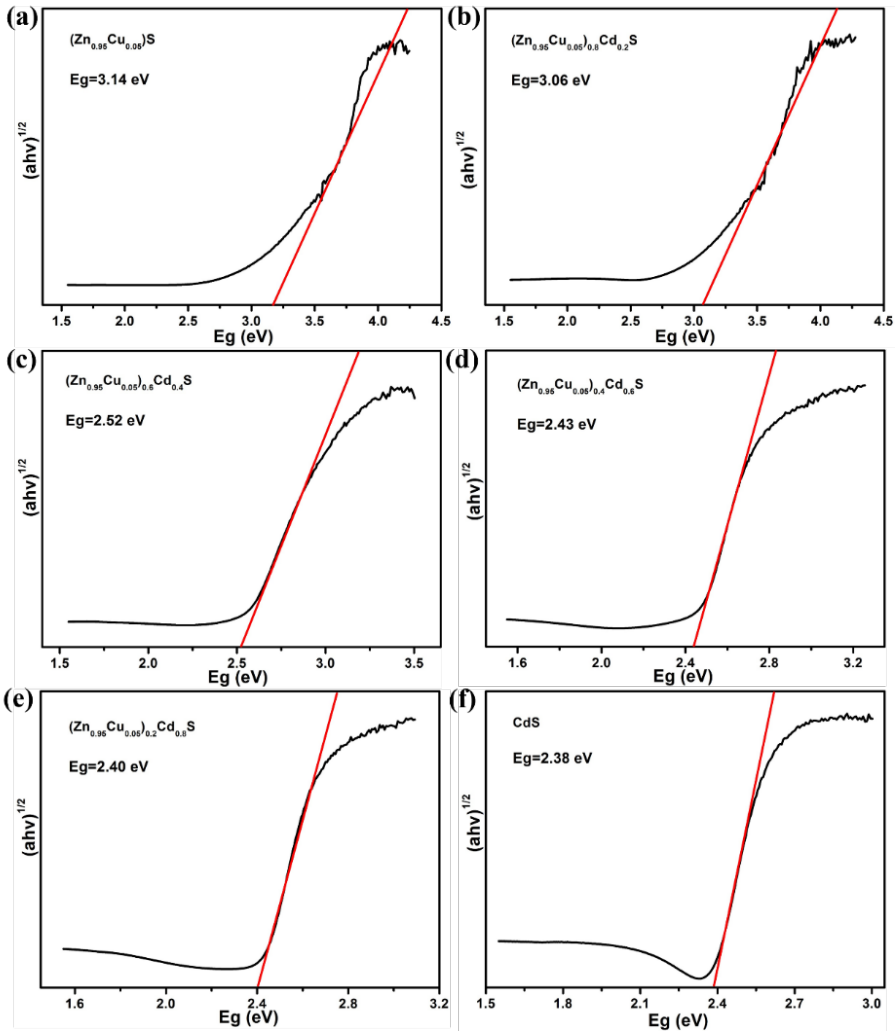

Figure S19 The bandgaps of $(Zn_{0.95}Cu_{0.05})S$ (a), $(Zn_{0.95}Cu_{0.05})_{0.8}Cd_{0.2}S$ (b), $(Zn_{0.95}Cu_{0.05})_{0.6}Cd_{0.4}S$ (c), $(Zn_{0.95}Cu_{0.05})_{0.4}Cd_{0.6}S$ (d), $(Zn_{0.95}Cu_{0.05})_{0.2}Cd_{0.8}S$ (e) and CdS (f) calculated according to the Kubelka-Munk (KM) method.

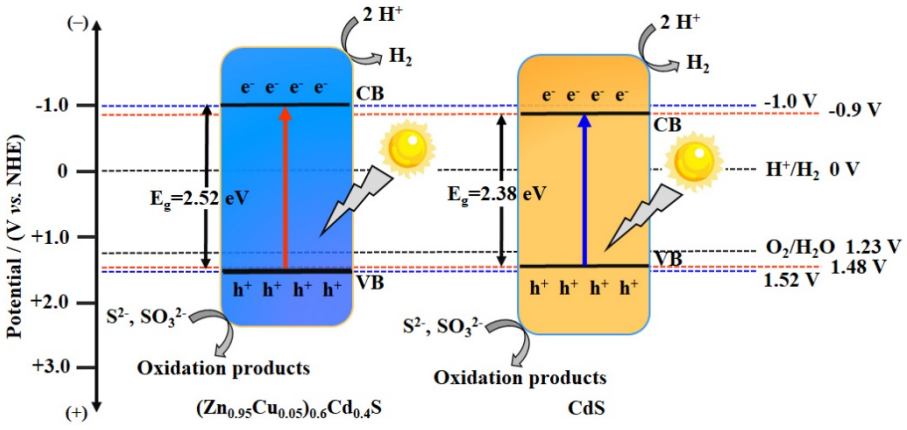

Figure S20 Mechanism of $(Zn_{0.95}Cu_{0.05})_{0.6}Cd_{0.4}S$ and CdS for photocatalytic hydrogen production.

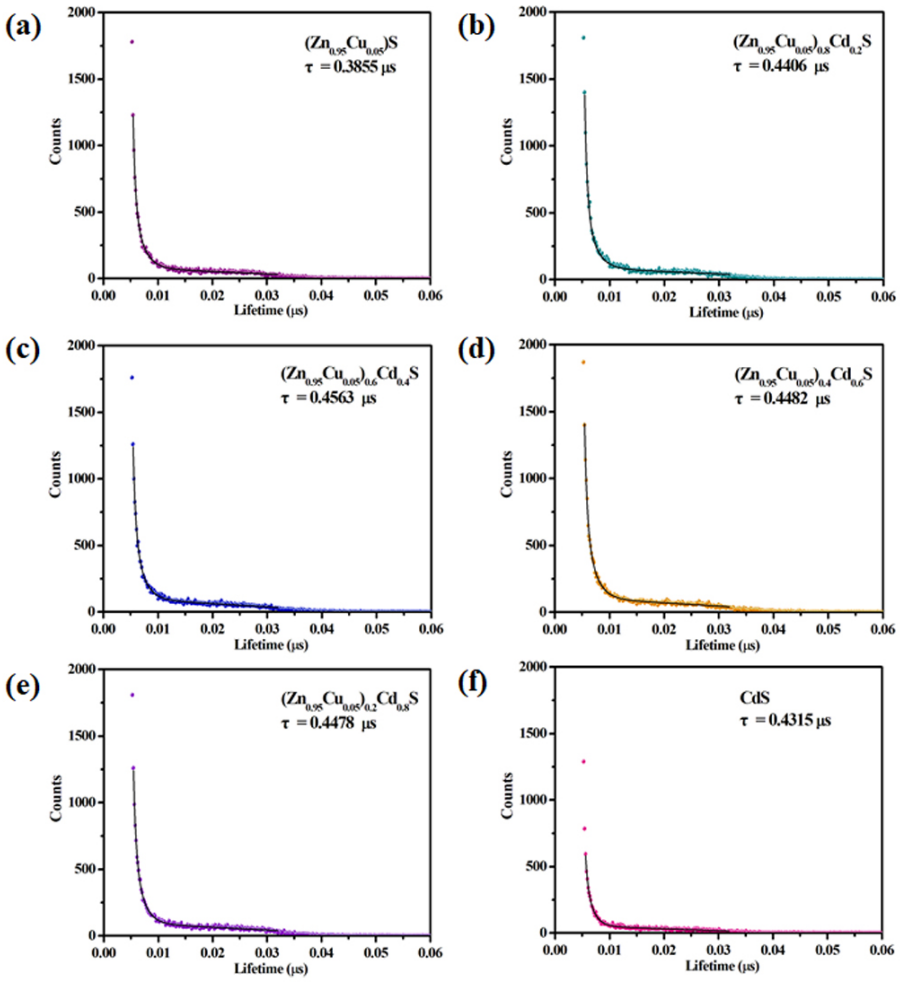

Figure S21 Decay curves and luminescent lifetimes of $(Zn_{0.95}Cu_{0.05})S$ (a), $(Zn_{0.95}Cu_{0.05})_{0.8}Cd_{0.2}S$ (b), $(Zn_{0.95}Cu_{0.05})_{0.6}Cd_{0.4}S$ (c),$(Zn_{0.95}Cu_{0.05})_{0.4}Cd_{0.6}S$ (d), $(Zn_{0.95}Cu_{0.05})_{0.2}Cd_{0.8}S$ (e) and CdS (f).

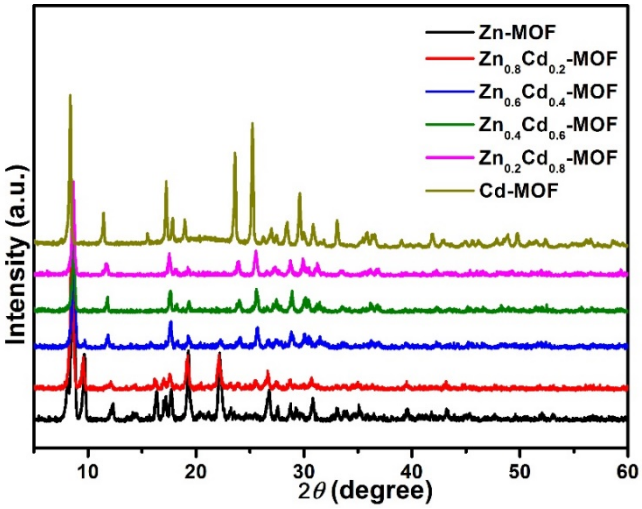

Figure S22 PXRD patterns of $(Zn_{1-x}Cd_x)$-MOF (x=0, 0.2, 0.4, 0.6, 0.8, 1.0).

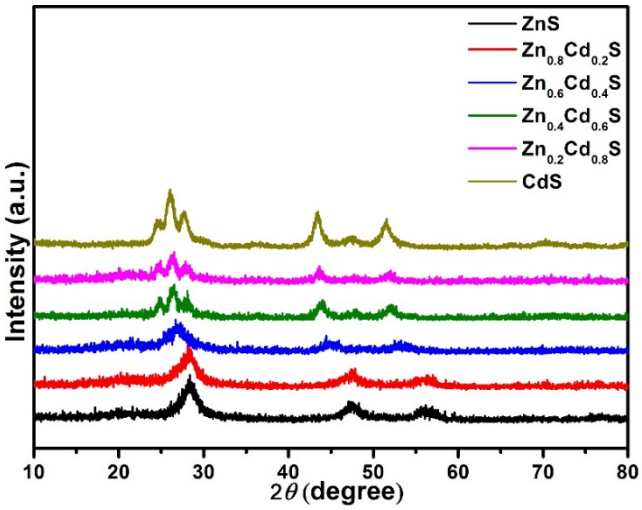

Figure S23 PXRD patterns of $(Zn_{1-x}Cd_x)S$ solid solutions (x=0, 0.2, 0.4, 0.6, 0.8, 1.0).

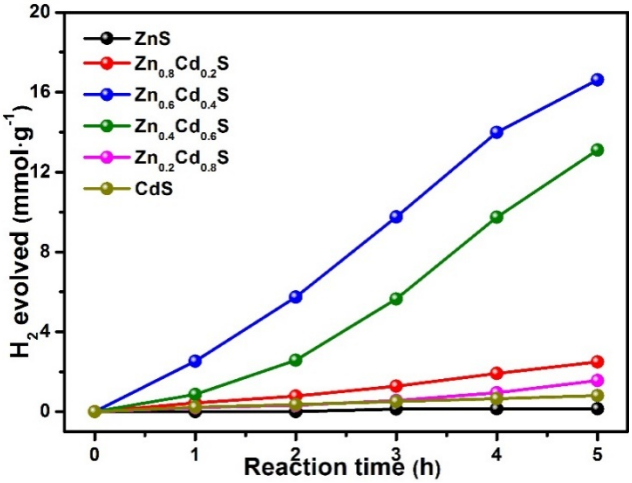

Figure S24 Photocatalytic performance of $(Zn_{1-x}Cd_x)S$ solid solutions.

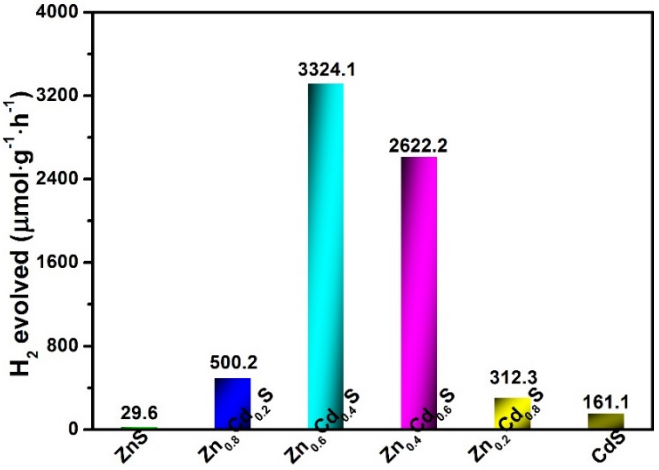

Figure S25 Comparison of photocatalytic HER of $(Zn_{1-x}Cd_x)S$ solid solutions.

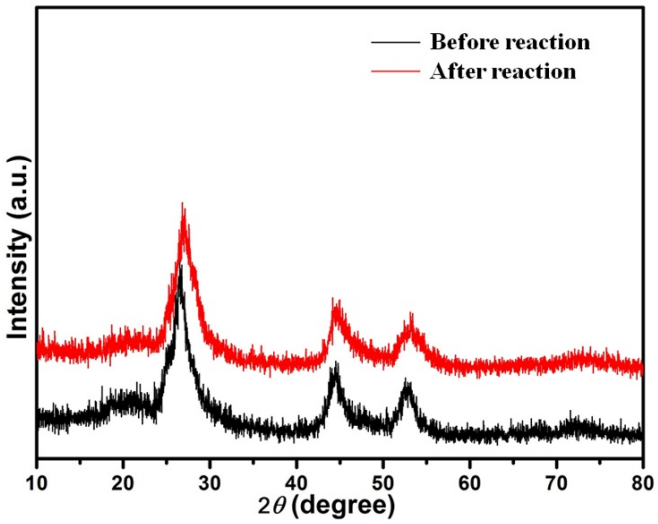

Figure S26 XRD patterns of $(Zn_{0.95}Cu_{0.05})_{0.6}Cd_{0.4}S$ collected after photocatalytic hydrogen evolution experiment.

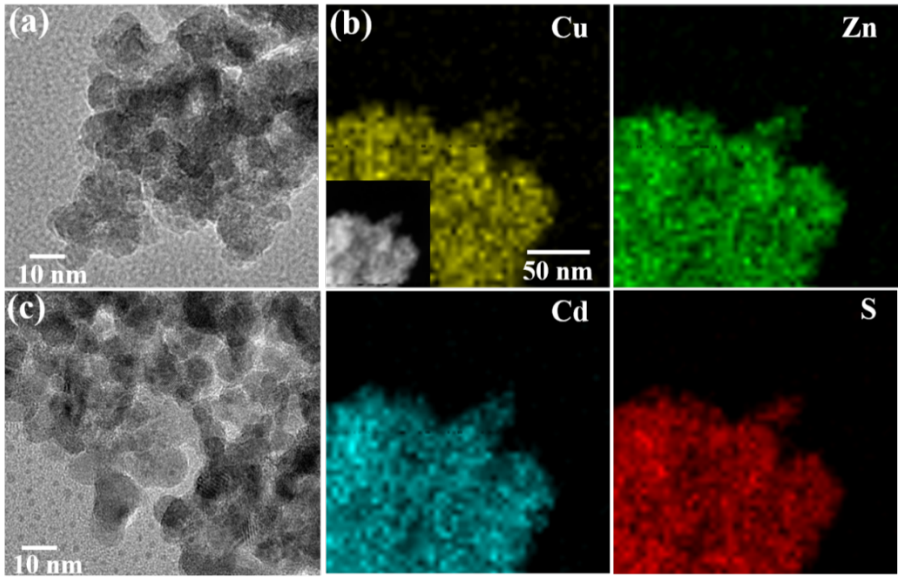

Figure S27 (a) TEM image of $(Zn_{0.95}Cu_{0.05})_{0.6}Cd_{0.4}S$before reaction, (b) elemental mapping images, and (c) TEM image of $(Zn_{0.95}Cu_{0.05})_{0.6}Cd_{0.4}S$ collected after photocatalytic hydrogen evolution experiment.

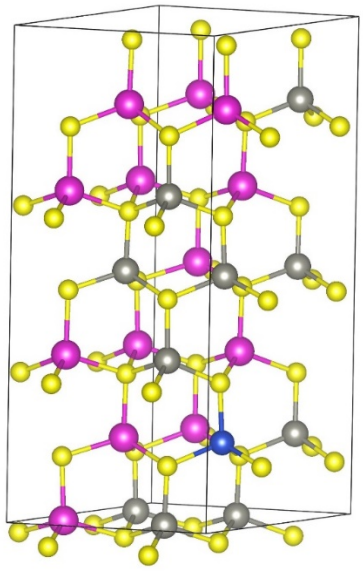

Figure S28 Solid solution model of $(Zn_{0.95}Cu_{0.05})_{0.6}Cd_{0.4}S$ (grey: Zn, blue: Cu, pink: Cd, yellow: S).

Table S1. The experimental data of inductively coupled plasma optical emission spectrometry (ICP-OES) and elemental analyses of $(Zn_{0.95}Cu_{0.05})_{1-x}Cd_xS$ solid solutions.

Sample	Weight percentage (wt %)					Atomic percentage (at %)				
	Zn	Cu	Cd	S	C	Zn	Cu	Cd	S	C
$(Zn_{0.95}Cu_{0.05})S$	52.80	4.37	-	35.86	6.97	31.62	2.63	-	43.46	22.29
$(Zn_{0.95}Cu_{0.05})_{0.8}Cd_{0.2}S$	49.00	4.31	6.72	32.74	7.23	31.11	2.54	2.40	40.95	23.00
$(Zn_{0.95}Cu_{0.05})_{0.6}Cd_{0.4}S$	21.70	2.58	51.7	20.83	3.19	19.41	2.27	26.14	37.5	14.68
$(Zn_{0.95}Cu_{0.05})_{0.4}Cd_{0.6}S$	5.97	1.42	69.90	21.34	1.37	6.61	1.30	40.91	43.99	7.19
$(Zn_{0.95}Cu_{0.05})_{0.2}Cd_{0.8}S$	2.58	0.47	75.30	20.73	0.92	2.78	0.48	46.50	44.97	5.27
CdS	-	-	81.00	18.21	0.79	-	-	53.21	41.99	4.80

Table S2 The energy positions of conduction and valence bands of samples. (ECB based on Mott-Schottky plots)

Sample	Eg (eV)	ECB (vs. NHE)	EVB (vs. NHE)
$(Zn_{0.95}Cu_{0.05})S$	3.14	-1.11	2.03
$(Zn_{0.95}Cu_{0.05})_{0.8}Cd_{0.2}S$	3.06	-1.22	1.84
$(Zn_{0.95}Cu_{0.05})_{0.6}Cd_{0.4}S$	2.52	-1.00	1.52
$(Zn_{0.95}Cu_{0.05})_{0.4}Cd_{0.6}S$	2.43	-1.38	1.05
$(Zn_{0.95}Cu_{0.05})_{0.2}Cd_{0.8}S$	2.40	-1.31	1.09
CdS	2.38	-0.50	1.88

Table S3. Comparison of the H_2-production rates of CuS_x cocatalysts solid solution for water splitting

Catalysts	Light source	Photocatalytic reactions	Activity $\mu mol \cdot h^{-1} \cdot g^{-1}$	AQE	Stability	Ref
$CuS/Cd_{0.4}Zn_{0.6}S$	(300 W Xe) > 420 nm	S^{2-}/SO_3^{2-}; None noble metal cocatalyst	1000	-	> 4 h	[5]
$Cu_{1.94}S\text{-}Zn_{0.23}Cd_{0.77}S$	(300 W Xe) > 420 nm	S^{2-}/SO_3^{2-}; None noble metal cocatalyst	7735	26.4% at 420nm	<20 h	[6]
$CuS/Zn_{0.8}Cd_{0.2}S$	(500 W Xe)	S^{2-}/SO_3^{2-}; None noble metal cocatalyst	2792	36.7% at 420 nm	-	[7]
$(Zn_{0.95}Cu_{0.05})_{0.6}Cd_{0.4}S$	(300 W Xe) > 420 nm	S^{2-}/SO_3^{2-}; None noble metal cocatalyst	4150.1	7.91% at 420nm	> 40 h	This work

Table S4. Comparison of the H_2-production rates of CdS-based solid solution for water splitting

Catalysts	Light source	Photocatalytic reactions	Activity $\mu mol \cdot h^{-1} \cdot g^{-1}$	AQE	Stability	Ref
$Cd_{0.5}Zn_{0.5}S$ nanorod	(300 W Xe) > 430 nm	S^{2-}/SO_3^{2-}; None noble metal cocatalyst	2580	62% at 425 nm	28 h	[8]
1D $Cd_{0.8}Zn_{0.2}S$	(300 W Xe) > 400 nm	S^{2-}/SO_3^{2-}; DMF	157.46	-	<12 h	[9]
$Zn_{0.5}Cd_{0.5}S$ porous nanosheets	(300 W Xe) > 420 nm	S^{2-}/SO_3^{2-}; None noble metal cocatalyst	1667	-	15 h	[10]
$Cd_{0.5}Zn_{0.5}S$	(300 W Xe) > 430 nm	S^{2-}/SO_3^{2-}; None noble metal cocatalyst	1790	43% at 420 nm	30 h	[11]
Hollow $Zn_{0.6}Cd_{0.4}S$ cages	(300 W Xe) > 420 nm	S^{2-}/SO_3^{2-}; None noble metal cocatalyst	5680	-	30 h	[12]
$Zn_{0.5}Cd_{0.5}S$	(350 W Xe) > 400 nm	S^{2-}/SO_3^{2-}; None noble metal cocatalyst	7420	9.6% at 420 nm	-	[13]
$ZnS/Zn_{1-x}Cd_xS/CdS$	(300 W Xe) > 420 nm	S^{2-}/SO_3^{2-}; None noble metal cocatalyst	106500	-	60 h	[14]
$Zn_{0.5}Cd_{0.5}S/PdP_{\sim 0.33}S_{\sim 1.67}$	(300 W Xe) > 420 nm	ascorbic acid; None noble metal cocatalyst	372120	19.7% at 420 nm	50 h	[15]
Ni^{2+}-doped $Zn_xCd_{1-x}S$	(300 W Xe) > 420 nm	S^{2-}/SO_3^{2-}; None noble metal cocatalyst	18820	22.8% at 420 nm	4 h	[16]
$NiS/Zn_{0.5}Cd_{0.5}S$/RGO	AM1.5, 100 mW cm^{-2}	S^{2-}/SO_3^{2-}; None noble metal cocatalyst	7514	31.1% at 420 nm	12 h	[17]
NiS-$Zn_{0.8}Cd_{0.2}S$	(300 W Xe) ≥ 420 nm	Triethanolamine; None noble metal cocatalyst	2507	-	9 h	[18]
$Ni(OH)_2$-$Zn_{0.8}Cd_{0.2}S$	(300 W Xe) ≥ 420 nm	Triethanolamine; None noble metal cocatalyst	7160	29.5% at 420 nm	9 h	[18]
Ni-$Zn_{0.8}Cd_{0.2}S$	(300 W Xe) ≥ 420 nm	Triethanolamine; None noble metal cocatalyst	3242	-	9 h	[18]
NiO-$Zn_{0.8}Cd_{0.2}S$	(350 W Xe) ≥ 420 nm	Triethanolamine; None noble metal cocatalyst	117	-	9 h	[18]
$NiS/Zn_{0.5}Cd_{0.5}S$	(300 W Xe) > 420 nm	S^{2-}/SO_3^{2-}; None noble metal cocatalyst	16780	-	> 20 h	[19]
1T-1$Li_xMoS_2/Cd_{0.5}Zn_{0.}$	(300 W Xe)	S^{2-}/SO_3^{2-};	7699	-	20 h	[20]

$_5$S	≥ 420 nm	None noble metal cocatalyst				
$MoS_2/Mn_{0.5}Cd_{0.5}S$	(300 W Xe)	S^{2-}/SO_3^{2-};	3938	-	12 h	[21]
	> 420 nm	None noble metal cocatalyst				
$PdS/Mn_{0.5}Cd_{0.5}S$	(300 W Xe)	S^{2-}/SO_3^{2-};	12280	-	<12 h	[21]
	> 420 nm	None noble metal cocatalyst				
$Cu_xS/Mn_{0.5}Cd_{0.5}S$	(300 W Xe)	S^{2-}/SO_3^{2-};				
(1≤x≤2)	> 420 nm	None noble metal cocatalyst	6940	-	12 h	[21]
$MoS_2/Mn_{0.25}Cd_{0.75}S$	(300 W Xe)	S^{2-}/SO_3^{2-};	12470	2.37% at	<24 h	[22]
	> 400 nm	None noble metal cocatalyst		420 nm		
Cu-doped $Zn_{0.5}Cd_{0.5}S$	(300 W Xe)	S^{2-}/SO_3^{2-};	21400	18.8% at	<9h	[23]
	≥ 420 nm	None noble metal cocatalyst		428 nm		
$Cd_{0.1}Cu_{0.01}Zn_{0.89}S$	(350 W Xe)	S^{2-}/SO_3^{2-};	1167	9.6% at	10 h	[24]
	≥ 430 nm	None noble metal cocatalyst		420 nm		
$(Zn_{0.95}Cu_{0.05})_{0.67}Cd_{0.33}S$	(300 W Xe)	S^{2-}/SO_3^{2-};	1693	15.7% at	<12 h	[25]
	≥ 420 nm	None noble metal cocatalyst		420 nm		
$(Zn_{0.95}Cu_{0.05})_{0.6}Cd_{0.4}S$	(300 W Xe)	S^{2-}/SO_3^{2-};	4150.1	7.91% at	> 40 h	This
	> 420 nm	None noble metal cocatalyst		420 nm		work

Reference:

(1) Huo, J. P.; Zeng, H. P. Copper Nanoparticles Embedded in the Triphenylamine Functionalized Bithiazole-metal Complex as Active Photocatalysts for Visible Light-driven Hydrogen Evolution. *J. Mater. Chem. A* **2015**, *3*, 17201-17208.

(2) Blöchl, P. E. Projector Argumented-wave Method. *Phys. Rev. B: Solid State* **1994**, *50*, 17953-17979.

(3) Perdew, J. P.; Burke, K.; Ernzerhof, M. Generalized Gradient Approximation Made Simple. *Phys. Rev. Lett*. **1996**, *77*, 3865-3868.

(4) Monkhorst, H. J.; Pack, J. D. Special Points for Brillouin-zone Integrations. *Phys. Rev. B: Solid State* **1976**, *13*, 5188.

(5) Wang, J.; Li, B.; Chen, J. Z.; Li, N.; Zheng, J. F.; Zhao, J. H.; Zhu, Z. P. Enhanced Photocatalytic H_2-production Activity of $Cd_xZn_{1-x}S$ Nanocrystals by Surface Loading MS (M = Ni, Co, Cu) Species. *Appl. Surf. Sci.* **2012**, *259*, 118-123.

(6) Chen, Y.; Zhao, S.; Wang, X.; Peng, Q.; Lin, R.; Wang, Y.; Shen, R.; Cao, X.; Zhou, G.; Li, J.; Xia, A.; Li, Y. Synergetic Integration of $Cu_{1.94}S$-$Zn_xCd_{1-x}S$ Heteronanorods for Enhanced Visible-light-driven Photocatalytic Hydrogen Production. *J. Am. Chem. Soc*. **2016**, *138*, 4286-4289.

(7) Zhang L. J.; Jiang T. F.; Li S.; Lu Y. C.; Wang L. L.; Zhang X. Q.; Wang D. J.; Xie T. F. Enhancement of Photocatalytic H_2 Evolution on $Zn_{0.8}Cd_{0.2}S$ Loaded with CuS as Cocatalyst and Its Photogenerated Charge Transfer Properties. *Dalton Trans.* **2013**, 42, 12998-13003.

(8) Liu, M.; Jing, D.; Zhou, Z.; Guo, L. Twin-induced One-dimensional Homojunctions Yield High Quantum Efficiency for Solar Hydrogen Generation. *Nat. Commun.* **2013**, *4*, 2278.

(9) Han, Z.; Chen, G.; Li, C.; Yu, Y.; Zhou, Y. Preparation of 1D Cubic $Cd_{0.8}Zn_{0.2}S$ Solid-solution Nanowires Using Levelling Effect of TGA and Improved Photocatalytic H_2-production Activity. *J. Mater. Chem. A* **2015**, *3*, 1696-1702.

(10) Yu, Y.; Zhang, J.; Wu, X.; Zhao, W.; Zhang, B. Nanoporous Single-crystal-like $Cd_xZn_{1-x}S$ Nanosheets Fabricated by the Cation-exchange Reaction of Inorganic-organic Hybrid ZnS-amine with Cadmium Ions. *Angew. Chem., Int. Ed.* **2012**, *51*, 897-900.

(11) Liu, M.; Wang, L.; Lu, G. M.; Yao, X.; Guo, L. Twins in $Cd_{1-x}Zn_xS$ Solid Solution: Highly Efficient Photocatalyst for Hydrogen Generation from Water. *Energy Environ. Sci*. **2011**, *4*,

1372-1378.

(12) Chen, J. M.; Chen, J. Y.; Li, Y. W. Hollow ZnCdS Dodecahedral Cages for Highly Efficient Visible-light-driven Hydrogen Generation. *J. Mater. Chem. A* **2017**, *5*, 24116-24125.

(13) Li, Q.; Meng, H.; Zhou, P.; Zheng, Y.; Wang, J.; Yu, J.; Gong, J. $Zn_{1-x}Cd_xS$ Solid Solutions with Controlled Bandgap and Enhanced Visible-light Photocatalytic H_2-production Activity. *ACS Catal*. **2013**, *3*, 882-889.

(14) Li, K.; Chen, R.; Li, S. L.; Han, M.; Xie, S. L.; Bao, J. C.; Dai, Z. H.; Lan, Y. Q. Self-assembly of a Mesoporous ZnS/Mediating Interface/CdS Heterostructure with Enhanced Visible-light Hydrogen-production Activity and Excellent Stability. *Chem. Sci*. **2015**, *6*, 5263-5268.

(15) Song, J.; Zhao, H.; Sun, R.; Li, X.; Sun, D. An Efficient Hydrogen Evolution Catalyst Composed of Palladium Phosphorous Sulphide ($PdPB_{0.33}SB_{1.67}$) and Twin Nanocrystal $Zn_{0.5}Cd_{0.5}S$ Solid Solution with Both Homo- and Hetero-junctions. *Energy Environ. Sci*. **2017**, *10*, 225-235.

(16) Wang, Y. B.; Wu, J. C.; Zheng, J. W.; Jiang, R. R.; Xu, R. Ni^{2+}-doped $Zn_xCd_{1-x}S$ Photocatalysts from Single-source Precursors for Efficient Solar Hydrogen Production under Visible Light Irradiation. *Catal. Sci. Technol*. **2012**, *2*, 581-588.

(17) Zhang, J.; Qi, L. F.; Ran, J. R.; Yu, J. G.; Qiao, S. Z. Ternary NiS/$Zn_xCd_{1-x}S$/Reduced Graphene Oxide Nanocomposites for Enhanced Solar Photocatalytic H_2-production Activity. *Adv. Energy Mater*. **2014**, *4*, 1301925.

(18) Ran, J. R.; Zhang, J.; Yu, J. G.; Qiao, S. Z. Enhanced Visible-light Photocatalytic H_2 Production by $Zn_xCd_{1-x}S$ Modified with Earth-abundant Nickel-based Cocatalysts. *ChemSusChem* **2014**, *7*, 3426-3434.

(19) Zhao, X. X.; Feng, J. R.; Liu, J.; Shi, W.; Yang, G. M.; Wang, G. C.; Cheng, P. An Efficient, Visible-light-driven, Hydrogen Evolution Catalyst NiS/$Zn_xCd_{1-x}S$ Nanocrystal Derived from a Metal-organic Framework. *Angew. Chem. Int. Ed*. **2018**, *57*, 9790-9794.

(20) Du, H.; Guo, H. L.; Liu, Y. N.; Xie, X.; Liang, K.; Zhou, X.; Wang, X.; Xu, A. W. Metallic 1T-Li_xMoS_2 Cocatalyst Significantly Enhanced the Photocatalytic H_2 Evolution over $Cd_{0.5}Zn_{0.5}S$ Nanocrystals under Visible Light Irradiation. *ACS Appl. Mater. Interfaces* **2016**, *8*, 4023-4030.

(21) Zhai, H. S.; Liu, X. L.; Wang, P.; Huang, B. B.; Zhang, Q. Q. Enhanced Photocatalytic H_2 Production of $Mn_{0.5}Cd_{0.5}S$ Solid Solution through Loading Transition Metal Sulfides XS (X = Mo, Cu, Pd) Cocatalysts. *Appl. Surf. Sci.* **2018**, *430*, 515-522.

(22) Huang, Q. Z.; Xiong, Y.; Zhang, Q.; Yao, H. C.; Li, Z. J. Noble Metal-free MoS_2 Modified $Mn_{0.25}Cd_{0.75}S$ for Highly Efficient Visible-light Driven Photocatalytic H_2 Evolution. *Appl. Catal. B: Environ.* **2017**, *209*, 514-522.

(23) Mei, Z.; Zhang, B.; Zheng, J.; Yuan, S.; Zhuo, Z.; Meng, X.; Chen, Z.; Amine, K.; Yang, W.; Wang, L.; Wang, W.; Wang, S.; Gong, Q.; Li, J.; Liu, F.; Feng, P. Tuning Cu Dopant of $Zn_{0.5}Cd_{0.5}S$ Nanocrystals Enables High-performance Photocatalytic H_2 Evolution from Water Splitting under Visible-light Irradiation. *Nano Energy* **2016**, *26*, 405-416.

(24) Liu, G. J.; Zhao, L.; Ma, L. J.; Guo, L. J. Photocatalytic H_2 Evolution under Visible Light Irradiation on a Novel $Cd_xCu_yZn_{1-x-y}S$ Catalyst. *Catal. Commun.* **2008**, *9* 126-130.

(25) Zhang, W.; Zhong, Z.; Wang, Y.; Xu, R. Doped Solid Solution: $(Zn_{0.95}Cu_{0.05})_{1-x}Cd_xS$ Nanocrystals with High Activity for H_2 Evolution from Aqueous Solutions under Visible Light. *J. Phys. Chem. C* **2008**, *112*, 17635-17642.